CRITICAL STATE ANALYSIS OF GOLD MINE TAILINGS VIA ISOTROPICALLY CONSOLIDATED UNDRAINED COMPRESSION

Submitted by

Cameron R. Hale

Department of Civil and Environmental Engineering

In partial fulfillment of the requirements

For the Master of Science Degree

Colorado State University

Fort Collins, Colorado

April 2022

Committee:

Advisor: Christopher A. Bareither

Joseph Scalia IV

Sean Gallen

ABSTRACT

The focus of this project was to evaluate the undrained shear behavior of gold mine tailings from a mine in Central America. Consolidated undrained triaxial compression tests were performed. The tailings exhibited a tendency to contract followed by a phase transition and strain-hardening behavior. Tailings specimens were prepared via moist tamping and tested at four effective confining stresses: 50, 100, 200, and 400 kPa. A critical state analysis was performed that included three failure criterions: (i) peak excess pore pressure; (ii) peak deviator stress; and (iii) limiting strain at the end of shearing. Peak excess pore pressure developed in a range of 5-6% axial strain for all specimens, and shear strength at this criterion was characterized by an effective friction angle of 32° and an undrained shear strength ratio of 0.26 (ratio of undrained shear strength to vertical effective consolidation stress). Peak deviator stress occurred between 17% and 22% axial strain, and shear strength was characterized by an effective friction angle of 31° and an undrained shear strength ratio of 0.33. The limiting strain of the triaxial tests was 25% axial strain, and shear strength was characterized by an effective friction angle of 30° and an undrained shear strength ratio of 0.34. The small changes in effective stress friction angle and undrained shear strength ratio between axial strains ranging from 17% to 25% suggest the material reached critical state. Critical state lines created for each of the failure criterion were linear with respect to logarithm of average effective stress, and the difference between the critical state line at peak pore pressure versus peak deviator stress was approximately + 0.015 void ratio.

TABLE OF CONTENTS

LIST OF TABLES

LIST OF FIGURES

INTRODUCTION

As mineral resource demands rise and high-grade ore deposits are depleted, tailings engineering becomes increasingly important. Mine tailings are the leftover material from ore processing. Ore generally is crushed, pulverized, and then mixed with water and chemical reagents to extract the valuable minerals. The residue is mine tailings, which most commonly is in slurry form that must subsequently be managed safely with best available technologies. The slurry often is pumped through a device known as a hydro-cyclone to separate larger “sand-sized” particles that can be used for embankment construction while the remaining silty or clayey slurry (slimes) is deposited behind the embankment that serves as containment. This type of mine waste containment system is known as a tailings storage facility (TSF).

Tailings storage facilities exist at most mine sites across the world; some are completed, inactive sites while others are operating as active sites. When designed, constructed, and maintained properly, TSFs provide safe long-term tailings storage. However, proper design, construction, and maintenance are challenged by sequential construction that occurs throughout mine operations as TSFs are built gradually, lift by lift, as mine waste is produced. Construction of TSFs can last decades, and during that time, there commonly are rollovers in personnel such as design engineer, construction manager, or even mine owner. Each time responsibility of a TSF changes hands there is risk of knowledge about the TSF slipping through the cracks.

Tailings storage facilities also are challenging engineered structures due to the variability and low shear strength of slurry-deposited tailings. The majority of TSFs contain slurry-deposited tailings, which unfortunately have shown to have the potential for liquefaction flow failure if the embankments containing the tailings are compromised. Tailings consist mostly of silt with clay and sand but can have higher or lower clay contents depending on the ore body geology and milling process.

Catastrophic TSF failures have drawn attention to the use of filtered tailings as an alternative mine waste containment strategy. Tailings filtration involves removing sufficient moisture from the material such that material transitions from liquid-like to solid-like. Filtered tailings can be placed denser with less contained water than slurry tailings and are more structurally stable. Filtered tailings are placed in “lifts” that accumulate to form “stacks”. Although filtered tailings are arguably more desirable than slurry tailings deposition, shear strength of filtered tailings and understanding whether a filtered tailings stack will potentially exhibit dilative or contractive behavior during shear deformation is critical to design.

The objective of this project was to evaluate the undrained shear behavior of filtered tailings from a gold mine in Central America. The mine has used filtered tailings and there is a desire to understand placement conditions of the tailings that can lead to dilative states throughout the lifecycle of the tailings facility. Isotropically-consolidated undrained triaxial compression tests were performed on the filtered gold tailings to assess the shear behavior for a loosely compacted material and identify the critical state line.

MATERIALS AND METHODS

Isotropically consolidated undrained triaxial compression tests (ASTM D4767) were performed on filtered tailings from a gold mine in Central America. Appendix A contains pictures of the material before, during, and after triaxial testing. Characteristics of the mine tailings are summarized in Table 1. All characterization testing was conducted in accordance with ASTM standards as described in Gorakhki et al. (2021). The tailings were predominantly fine-grained (> 85%) and contained more than 23% clay-sized particles (< 0.002 mm). The high fines content and presence of clay-sized particles yielded a liquid limit of 30 and plasticity index of 9 that classified the tailings as a lean clay (CL).

All tailings samples were sterilized via oven drying upon receipt at Colorado State University. After sterilization, the oven-dried material was broken up, passed through a No. 4 sieve (4.75 mm), and mixed thoroughly prior to triaxial testing. All oven-dried tailings used for triaxial testing were moisture conditioned to 5% water content, mixed thoroughly, and left in a sealed container overnight to equilibrate.

Triaxial test specimens were prepared via moist tamping to achieve looser particle fabrics that have the tendency to contract and reach critical state during undrained shear. All testing was conducted on 71-mm diameter specimens prepared in a split mold within a 0.25-mm thick latex membrane. A target specimen density corresponding to 80% of standard effort maximum dry density (1.69 g/cm^3 in Table 1) was achieved via compacting in 10 lifts of equal mass as outlined by Reid et al. (2022). An undercompaction ratio of 5% was used in the specimen preparation procedure (Ladd 1978). The undercompaction corresponds to lower compacted lift densities progressing from the bottom to the top of the specimen.

The specimen shape and compacted density were maintained during removal of the split-mold and filling the cell with water via tracing paper wrapped around the outside of the membrane. Tracing paper cut to appropriate dimensions was wrapped around the membrane and secured with low-adhesive tape prior to compacting the specimen within the split mold. The tracing paper prevented the loosely compacted tailings from sloughing between split-mold removal and application of cell pressure. Water within the triaxial cell removed the adhesion of the tape on the tracing paper, which separated the tracing paper from around the membrane prior to shearing (Jerhing and Bareither 2015; Borja et al. 2020).

An initial low effective consolidation stress of approximately 7 kPa was applied on the test specimens and maintained during the saturation phase. Specimen saturation was assumed complete once B-values > 0.95 were achieved (ASTM D4767). Subsequently, the cell pressure was increased to the target effective confining stress and specimens were consolidated for at least 24 hours prior to shearing. Complete consolidation was verified by observing no change in the out-flow water level during a period of at least 8 hours.

Specimens were isotropically consolidated to target effective confining stresses of 50 kPa, 100 kPa, 200 kPa, and 400 kPa, and then sheared undrained. Triaxial test parameters are summarized in Table 2. Undrained shearing was achieved via axial compression at a controlled axial strain rate of 1% per hour to a maximum axial strain of 25%. Testing was performed using a GEOTAC Sigma-1 Automated Load Test System. Prior to testing, all instruments were calibrated (see Appendix B) and calibration factors were entered into the Sigma-1 software.

The end-of-test specimen freezing technique was used to determine specimen void ratios (e.g., Reid et al. 2020). After shearing was completed, the cylinder containing the cell water was removed, along with the tracing paper and tape. The test specimen remained in-place with all valves closed to prevent water loss from the specimen prior to freezing. The specimen and triaxial base stand were placed in the freezer for up to 24 hours (Reid et al. 2020). The specimen was then removed from the freezer and the O-rings, top platen, and bottom platen were removed. The membrane was quickly and carefully removed by placing the sample vertically on a plastic cylinder and pulling the membrane downwards, allowing the membrane to separate from the still-frozen specimen. Cutting the membrane made membrane removal more difficult, as the thin 0.25 mm-thick latex membrane tended to tear and leave small pieces stuck to the specimen. After successfully removing the membrane, porous stones and filter papers were removed and the mass of the frozen specimen was recorded. The specimens were then oven-dried at 105 °C for at least 24 hours to determine the dry mass of tailings solids. The void ratios of the final test specimens were computed via mass-volume relationships assuming complete saturation.

DATA PROCESSING AND ANALYSIS

Raw data from the Sigma-1 software were processed in a spreadsheet using the measured calibration factors (Appendix B). The spreadsheet was set up to compute various relevant factors, including but not limited to deviator stress, excess pore pressure, axial strain, principal stresses, and Skempton's A parameter. All test specimens were observed to physically deform to a parabolic shape during axial deformation (see pictures in Appendix A), such that a parabolic area correction factor was applied for stress calculations (Mulabdic 1993). Test data were processed to generate plots displaying relationships of deviator stress versus axial strain, excess pore pressure versus axial strain, principal effective stress ratio versus axial strain, and *q* versus *p'* (stress paths). The values of *q* and *p'* were computed in MIT convention as follows:

$$q = \frac{\sigma'_1 - \sigma'_3}{2} \tag{1}$$

$$p' = \frac{\sigma'_1 + \sigma'_3}{2} \tag{2}$$

where σ'_1 is the effective major principal stress and σ'_3 is the minor effective principal stress.

Brandon et al. (2006) report that the following failure criterions can be considered when evaluating undrained shear failure: (1) peak excess pore pressure; (2) peak deviator stress; (3) peak principal stress ratio; (4) Skempton's A parameter reaching zero (i.e., excess pore pressure equal to zero); (5) stress path reaching the K_f line (i.e., failure line in q-p' space); and (6) select limiting strain. Each failure criterion was considered, and the following observations were made regarding selecting or not selecting a given failure criterion:

- Peak excess pore pressure – *selected for analysis* – excess pore pressure ascended to a clear peak before descending, providing a clear transition point that could be used to define failure.
- Peak deviator stress – *selected for analysis* - data from all tests plateaued at a nearly constant deviator stress corresponding to 17% to 22% axial strain.

- Peak principal stress ratio – *not selected for analysis* – data fluctuations made determining the peak principal stress ratio difficult.
- Skempton's A parameter reaching zero – *not selected for analysis* – excess pore pressure did not reach zero during any of the tests, and thus, Skempton's A parameter did not reach zero.
- Stress path reaching the K_f line – *not selected for analysis* – the K_f line is dependent on the failure criterion selected to plot the K_f line. Different failure criterion can yield different K_f lines, which led to uncertainty in selecting the point at which the stress paths reached the K_f line.
- Limiting strain – *selected for analysis* – all tests were conducted to a maximum axial strain of 25%, providing a clear common point to identify failure.

Data from all tests were analyzed under the three selected failure criterions: (i) peak excess pore pressure; (ii) peak deviator stress; and (iii) select limiting strain. An effective stress friction angle and undrained shear strength were computed for each triaxial test under each criterion for comparison.

Duplicate triaxial tests were performed at each effective confining stress to ensure consistency. Tests were performed using three triaxial cells labeled "A", "B", and "C". The pair of triaxial tests conducted at an effective confining stress (σ'_c) of 50 kPa yielded nearly identical results. The pair of tests at σ'_c = 400 kPa also yielded nearly identical results. However, the duplicate tests for σ'_c = 100 kPa and σ'_c = 200 kPa did not compare identically to the original two triaxial tests at these two stress levels. The duplicate tests at σ'_c = 100 kPa and 200 kPa were the only tests performed using triaxial cell A, and upon closer inspection, a minor amount of rust was discovered in the piston bearing of triaxial cell A. The rust appeared to create inconsistent friction that resulted in erroneous load measurements that contrasted to the smooth axial load relationships of the other six tests.

The purpose of running duplicated triaxial tests at each confining stress was to verify the specimen preparation and test procedures used in this study. The 50 kPa and 400 kPa duplicated tests confirmed consistency. Furthermore, preliminary data analysis indicated that first set of triaxial tests at each of the four σ'_c (i.e., 50 ,100, 200, and 400 kPa) compared favorably to one another and agreed with anticipated undrained shear behavior of mine tailings (e.g., Reid et al. 2020) and silty soils (e.g., Brandon et al. 2006). Thus, the first triaxial tests at each σ'_c were selected for further assessment of shear strength and critical state, and the duplicate tests were not included. The remainder of this report focuses on the initial four triaxial tests performed at each confining stress.

RESULTS

Table 3 contains test results under three failure criterions: peak pore pressure, peak deviator stress, and limiting strain. Figures 1 through 4 display plots of various parameters vs axial strain for all tests. Figure 5 displays the stress paths for all tests. Figure 6 displays three critical state lines, one for each of the aforementioned failure criterion. Appendix C contains plots and data for each individual test.

For tailings specimens tested at σ'_c = 50, 100, 200, and 400 kPa, deviator stress increased rapidly until an axial strain of about 1% followed by a slower increase rate until an axial strain of approximately 20% (17%, 19%, 20%, and 22% respectively), from which point deviator stress remained relatively constant through the end of shearing (Figure 1).
For specimens tested at σ'_c = 50, 100, and 200 kPa, excess pore pressure increased rapidly until an axial strain of about 2% followed by a gradual decrease until an axial strain of approximately 20% (17%, 19%, and 20% respectively), from which point deviator stress remained relatively constant through the end of shearing (Figure 2). For the tailings specimen tested at σ'_c = 400 kPa, excess pore pressure also increased rapidly until an axial strain of about 2%, after which it decreased at a moderate rate until an axial strain of approximately 20%, followed by a slower rate of decrease through the end of shearing.

The principal effective stress ratio versus axial strain curves for specimens tested at σ'_c = 100, 200, and 400 kPa were generally similar whereby the principal effective stress ratio peaked at an A parameter of approximately 3.2 at approximately 8% axial strain followed by all three curves converging at an A parameter of 2.85 at the end of shearing (Figure 3). However, the principal effective stress ratio vs axial strain curve for the specimen tested at σ'_c = 50 kPa is different from the other three whereby it peaked at an A parameter of approximately 3.9 at approximately 8% axial strain and then decreased to an A parameter of approximately 3.2 at the end of shearing. The second 50 kPa test yielded an almost identical stress ratio plot to the first 50 kPa test, confirming the difference in stress ratios was not the result of errors during testing.

The 50 kPa test likely exhibited higher peak and final stress ratios because some dilation in the material was suppressed as the confining stress was increased to 100, 200, and 400 kPa for subsequent tests. Dilation suppression would also account for the 50 kPa test yielding higher secant friction angles than the other three tests at each failure criterion (Table 3).

Skempton's A parameter peaked at approximately 1.25 at approximately 3% axial strain for all tests, followed by a gradual descent to approximately 0.8 at approximately 20% axial strain for all tests (Figure 4). The four specimens yielded uniform stress path curvatures, with material contracting to and then following the Kf line (Figure 5).

For all four specimens, *p'* decreased during shearing, placing the specimens to the right of the critical state line and indicating that at 80% maximum dry density the material exhibited contractive, strain-hardening behavior. Three critical state lines are shown in Figure 6. The critical state line on the left represents the material at peak pore pressure (approximately 6% axial strain), the middle line represents the material at peak deviator stress (approximately 20% axial strain), and the right line represents the material at limiting strain (25% axial strain). The space between the peak deviator stress and limiting strain critical state lines is much smaller than the space between the peak excess pore pressure and peak deviator stress lines, indicating the material is very near or at critical state at peak deviator stress. Assuming the material reaches critical state at peak deviator stress yields a critical state friction angle of 31.0 degrees and a critical state undrained strength ratio of 0.33.

CONCLUSIONS

Isotropically consolidated undrained triaxial compression tests were conducted on gold mine tailings. Testing was conducted with the intent to determine the critical state shear strength and a unique critical state line. The following conclusions were drawn from this study:

- All triaxial test specimens prepared from the mine tailings at 80% maximum dry density exhibited a tendency to contract and yielded positive pore pressure during undrained shear in triaxial compression;
- The triaxial tests all reached peak excess pore pressure at approximately 5% to 6% axial strain;
- The triaxial tests all reached peak deviator stress at approximately 17% to 22% axial strain;
- The effective stress friction angle and undrained shear strength ratio determined for each test exhibited negligible change between the axial strain at which peak deviator stress was reached (17%-22%) and the limiting axial strain of 25%, which suggests that a unique critical state was achieved in the triaxial tests;
- The assumed critical state identified at peak deviator stress yielded a critical state friction angle of 31° and an undrained shear strength ratio of 0.33.

REFERENCES

ASTM D4767-11 (2011). *Standard Test Method for Consolidated Undrained Triaxial Compression Test for Cohesive Soils*, ASTM International, West Conshohocken, PA.

Borja, R.N., Bareither, C.A. (2020). Shear Behavior of Waste Rock and Filtered Tailings. *Geo-Congress*, *GSP,* 1339-1354.

Brandon, T.L., Rose, A.T., Duncan, J.M. (2006). Drained and Undrained Strength Interpretation for Low-Plasticity Silts. *Journal of Geotechnical and Geoenvironmental Engineering, February 2006* , 250-257.

Gorakhki, M.H., Bareither, C.A., Scalia, J., Aparicio, M. (2021). Hydrologic and Environmental Behavior of GeoWaste and Waste Rock in Field Experimental Piles. *Mining, Metallurgy & Exploration*, 1339-1354.

Jehring, M.M., Bareither, C.A. (2016). Tailings Composition Effects on Shear Strength Behavior of Co-mixed Mine Waste Rock and Tailings. *Acta Geotechnica, 2016*, 11:1147-1166

Ladd, R.S. (1993). Area Correction in Triaxial Testing. *Geotechnical Testing Journal*, *GTODJ, Vol. 1, No. 1, March 1978*, 16-23.

Mulabdic, M. (1978). Preparing Test Specimens Using Undercompaction. *Swedish Geotechnical Institute, Varia 408, March 1993*, 16-23.

Reid, D., Fourie, A., Ayala, J.L., Dickinson, S., Ochoa-Cornejo, F., Fanni, R., Garfias, J., Viana Da Fonseca, A., Ghafghazi, M., Ovalle, C., Reimer, M., Rismanchian, A., Olivera, R., Suazo, G. (2020). Results of a Critical State Line Testing Round Robin Programme. *Geotechnique, July 2020* , 1-15.

Reid, D., Fanni, R., Fourie, A. (2022). Effect of Tamping Conditions on the Shear Strength of Tailings. *International Journal of Geomatics, Vol. 22, Issue 3, March 2022* , 04021288-1 – 04021288-10.

Table 1. Summary of material characteristics (modified from Gorakhki et al. 2021).

LL (%)	*PI* (%)	USCS	Gravel Content (%)	Sand Content (%)	Fines Content (%)	Clay-Size Content (%)	G_s	w_{opt} (%)	$\rho_{d,max}$ (g/cm^3)
30.1	9.2	CL	0	14.3	85.7	23.6	2.68	15.8	1.69

Notes: *LL* = liquid limit; *PI* = plasticity index; USCS = Unified Soil Classification System; clay-size content taken as percent particles by mass < 0.002 mm; G_s = specific gravity; w_{opt} = optimum water content and $\rho_{d,max}$ = maximum dry density determined from Standard-effort compaction tests.

Table 2. Summary of testing parameters

Test	Triaxial Compression
Conditions	Consolidated, Undrained
Sample Diameter	71 mm
Membrane Thickness	0.25 mm
Molding Water Content	5%
Compaction	80% of $\rho_{d,max}$
Undercompaction Ratio	5%
Number of Lifts	10
B Parameter	> 0.95
Strain Rate	1% / hour
Limiting Strain	25%

Table 3. Summary of tests results at various failure criterion

Failure Criterion	Target σ'_c (kPa)	σ'_c (kPa)	e	$\varepsilon_{a,f}$ (%)	σ'_{3f} (kPa)	σ'_{1f} (kPa)	$\Delta\sigma_f$ (kPa)	$u_{e,f}$ (kPa)	Su (kPa)	Su/σ'_c	Average Su/σ'_c	φ'_{sec} (º)	φ'_t (º)
Peak Excess Pore Pressure	50	47.16	0.74	5.8	10.6	40.3	29.7	36.6	12.6	0.27	0.26	35.7	32.1
	100	96.60	0.69	5.4	25.4	81.2	55.9	71.2	23.7	0.24		31.6	
	200	192.29	0.65	5.3	55.6	171.8	116.2	136.7	49.2	0.26		30.7	
	400	396.36	0.60	6.2	120.6	368.5	247.8	275.7	105.0	0.26		30.4	
Peak Deviator Stress	50	46.40	0.74	17.2	13.8	49.0	35.2	32.6	15.1	0.33	0.33	34.2	31.0
	100	96.32	0.69	18.6	34.8	106.9	72.1	61.5	30.9	0.32		30.6	
	200	193.52	0.65	20.3	78.0	231.2	153.2	115.5	65.6	0.34		29.7	
	400	396.17	0.60	21.6	158.6	467.0	308.4	237.6	132.2	0.33		29.5	
Limiting Strain	50	47.02	0.74	25.0	16.3	51.5	35.2	30.8	15.3	0.33	0.34	31.3	29.6
	100	96.70	0.69	25.0	39.4	113.5	74.1	57.3	32.2	0.33		29.0	
	200	193.40	0.65	25.0	83.0	238.1	155.1	110.5	67.4	0.35		28.9	
	400	395.06	0.60	25.0	163.1	469.9	306.8	232.0	133.4	0.34		29.0	

Notes: σ'_c = effective confining stress; e = void ratio; $\varepsilon_{a,f}$ = axial strain at failure; σ'_{3f} = minor effective principle stress at failure; σ'_{1f} = major effective principle stress at failure; $\Delta\sigma_f$ = deviator stress at failure; $u_{e,f}$ = excess pore pressure at failure; Su = undrained shear strength; φ'_{sec} = secant friction angle; φ'_t = tangent friction angle.

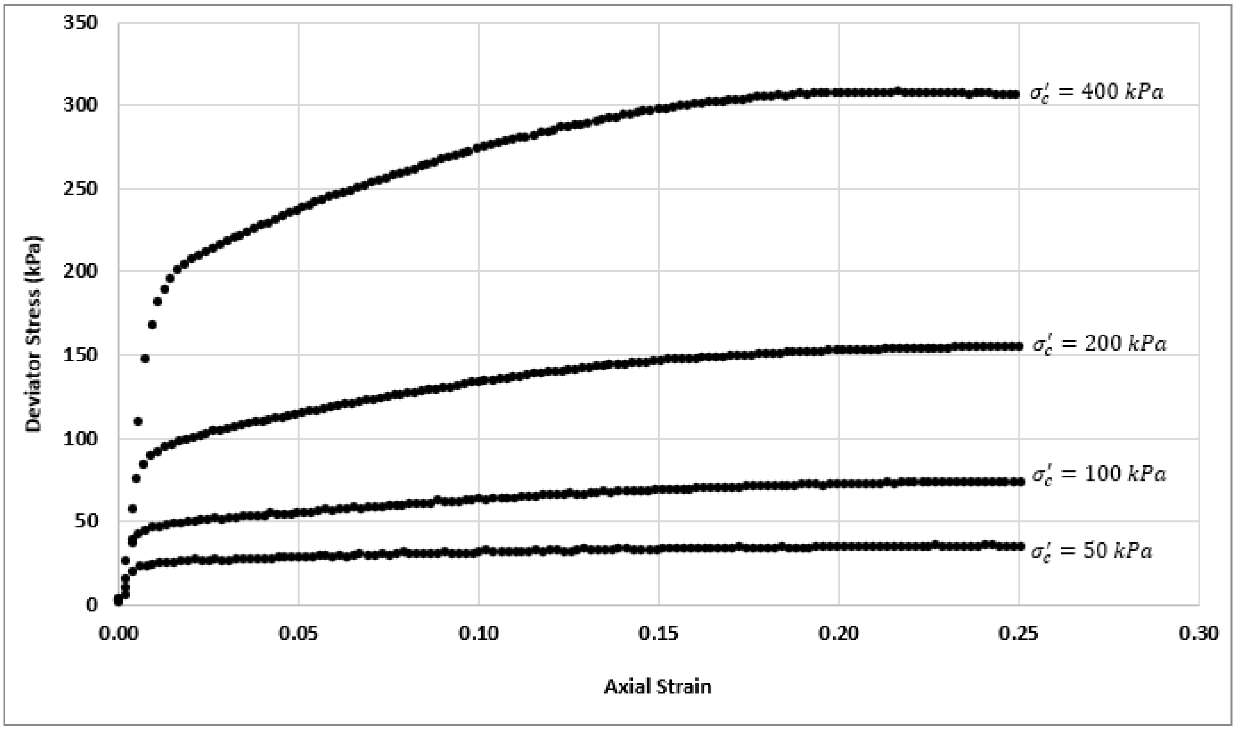

Fig. 1. Deviator Stress vs Axial Strain for Consolidated Undrained Triaxial Compression tests of filtered gold tailings.

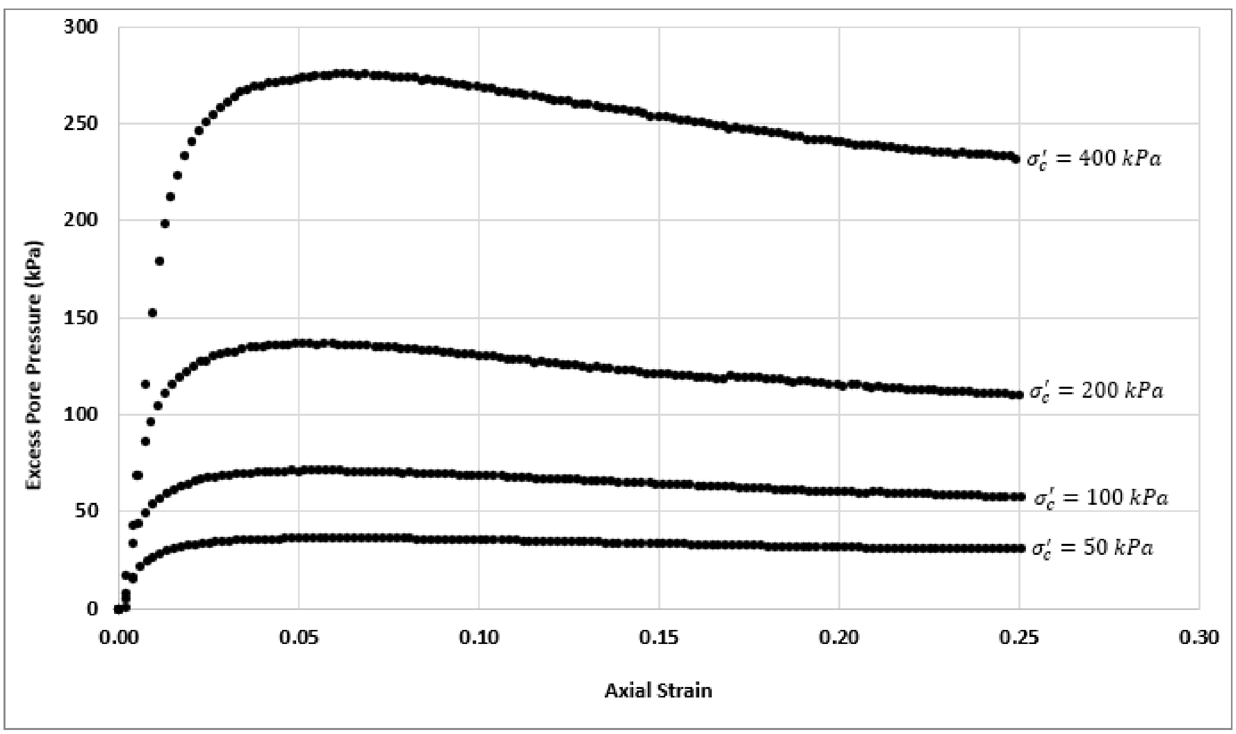

Fig. 2. Excess Pore Pressure vs Axial Strain for Consolidated Undrained Triaxial Compression tests of filtered gold tailings.

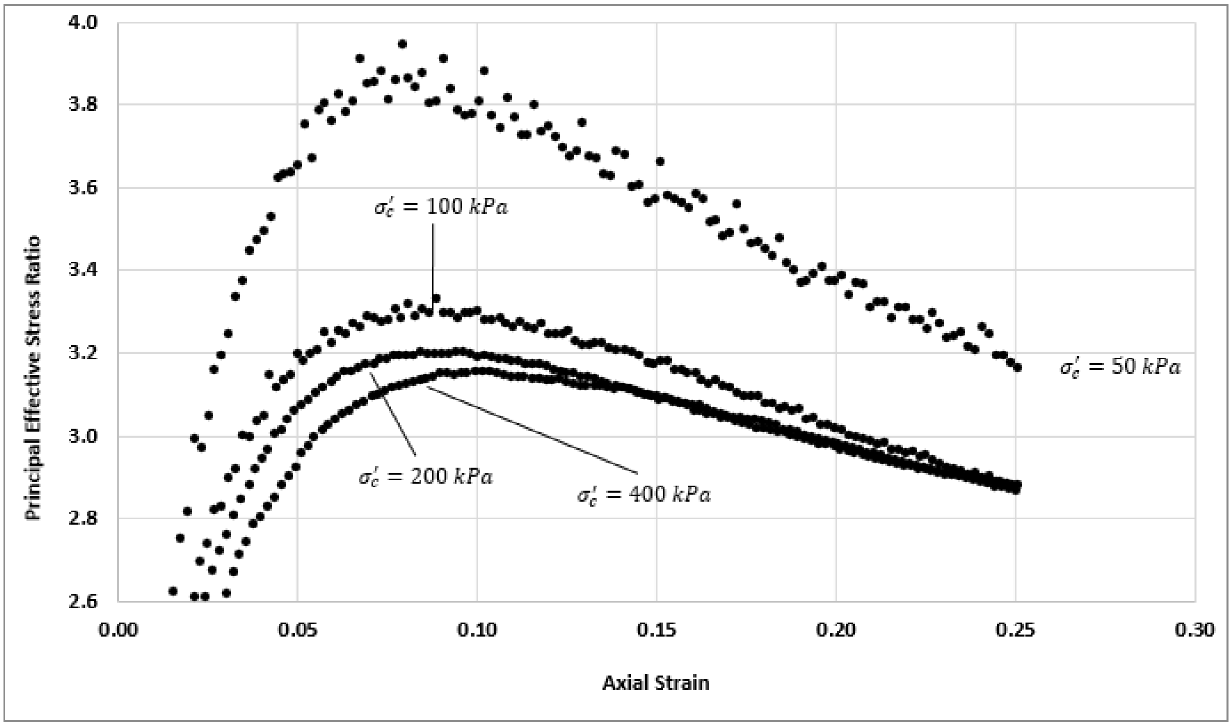

Fig. 3. Principal Effective Stress Ratio vs Axial Strain for Consolidated Undrained Triaxial Compression tests of filtered gold tailings.

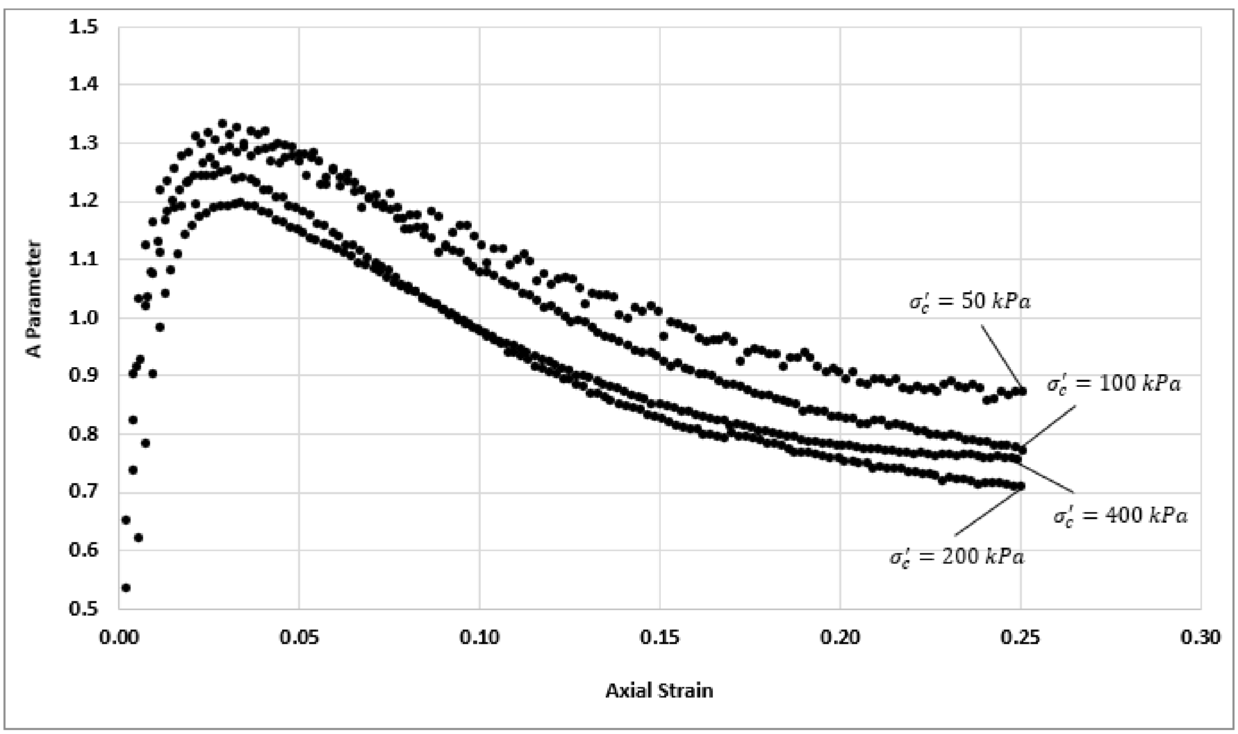

Fig. 4. Skempton's A Parameter vs Axial Strain for Consolidated Undrained Triaxial Compression tests of filtered gold tailings.

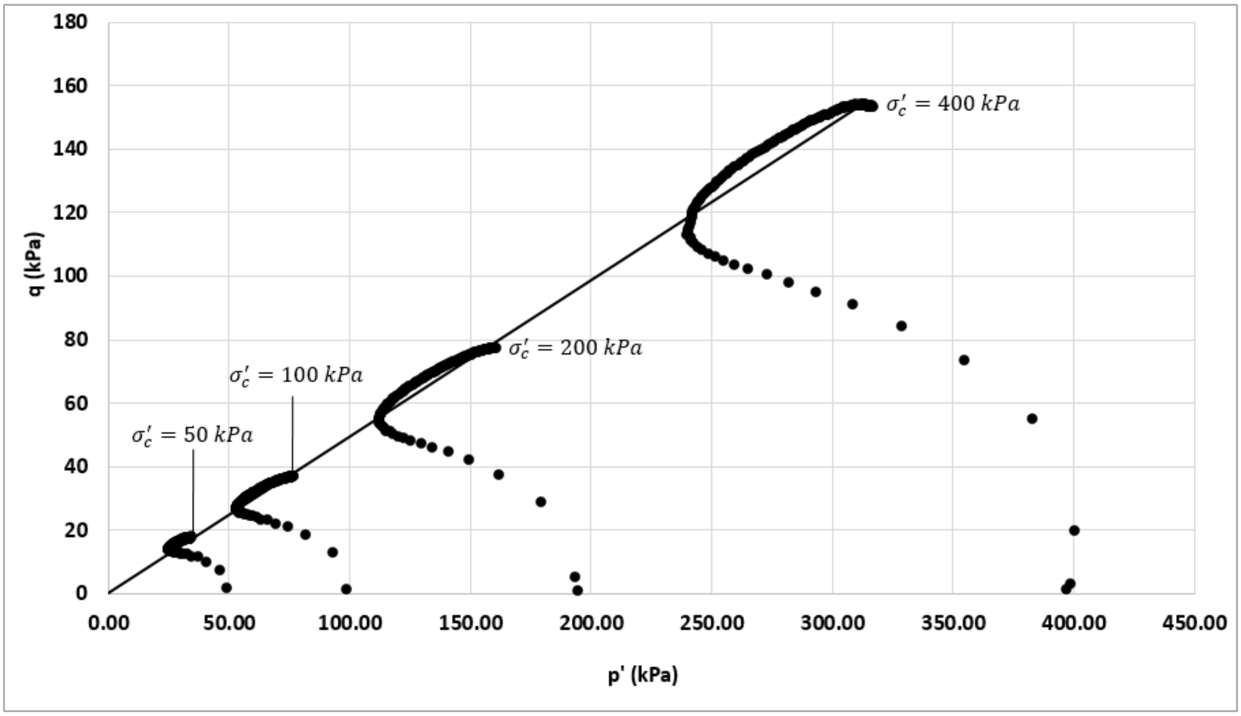

Fig. 5. Stress Paths for Consolidated Undrained Triaxial Compression tests of filtered gold tailings. Kf line generated with peak deviator stress as critical state failure criterion.

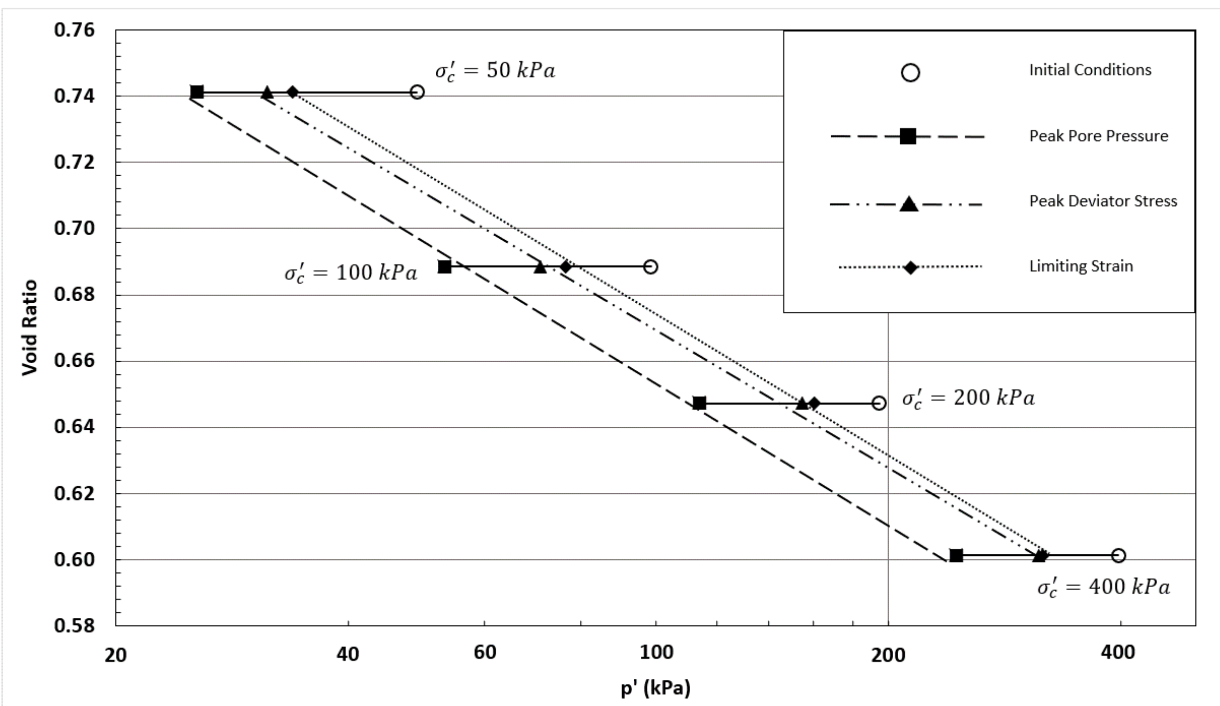

Fig. 6. Critical State Lines for Consolidated Undrained Triaxial Compression tests of filtered gold tailings at various failure criterion.

APPENDIX A: Pictures

Fig. A1. Tailings at 0% moisture content passing #4 Sieve.

Fig. A2. Sample preparation supplies.

Fig. A3. Samples were saturated and consolidated using a pressure panel (right) and sheared using a GEOJAC data acquisition system (left).

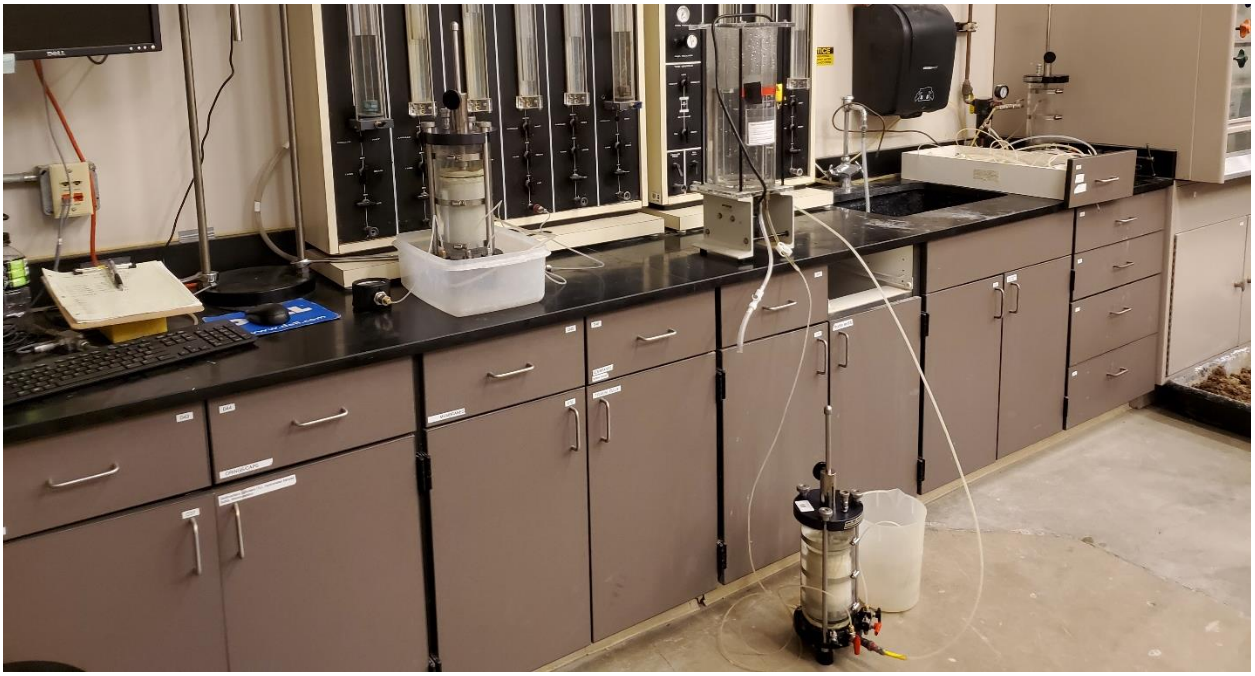

Fig. A4. A sample is inundated with de-aired water (bottom-right) while another is back-pressure saturated (top-left).

Fig. A5. A sample in a freezer.

Fig. A6. After shearing, freezing, and drying, the samples were observed to have undergone parabolic deformation.

APPENDIX B: Calibration plots and calibration factors

Table B1. Summary of calibration factors

Sensor (conversion unit)	Slope (m)	Excitation (Ve)	Calibration Factor (m*Ve)
Load Cell (N)	-280961.53493	10.0466	-2822708.15683
Displacement DCDT (mm)	-5.07658	10.0466	-51.00237
Pore Press. Transducer (kPa)	13503.82125	10.0466	135667.49057
Cell Press. Transducer (kPa)	6745.76929	10.0466	67772.04575

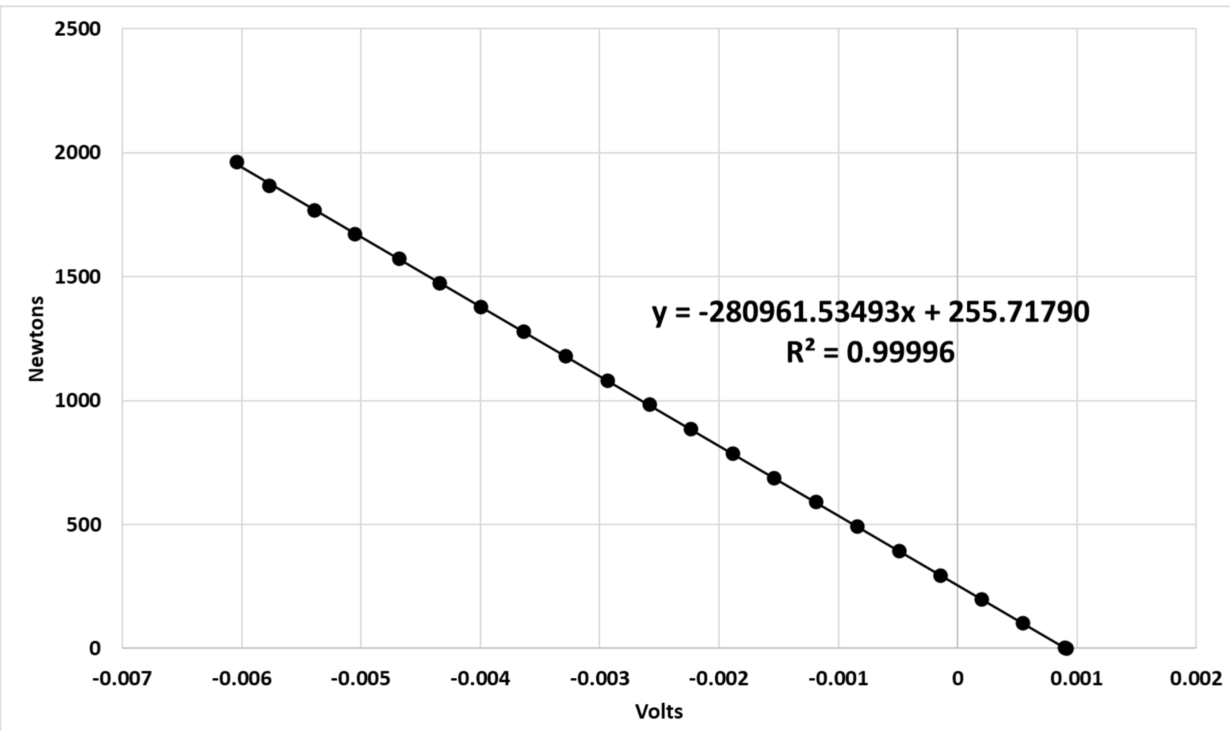

Fig. B1. Load sensor calibration plot.

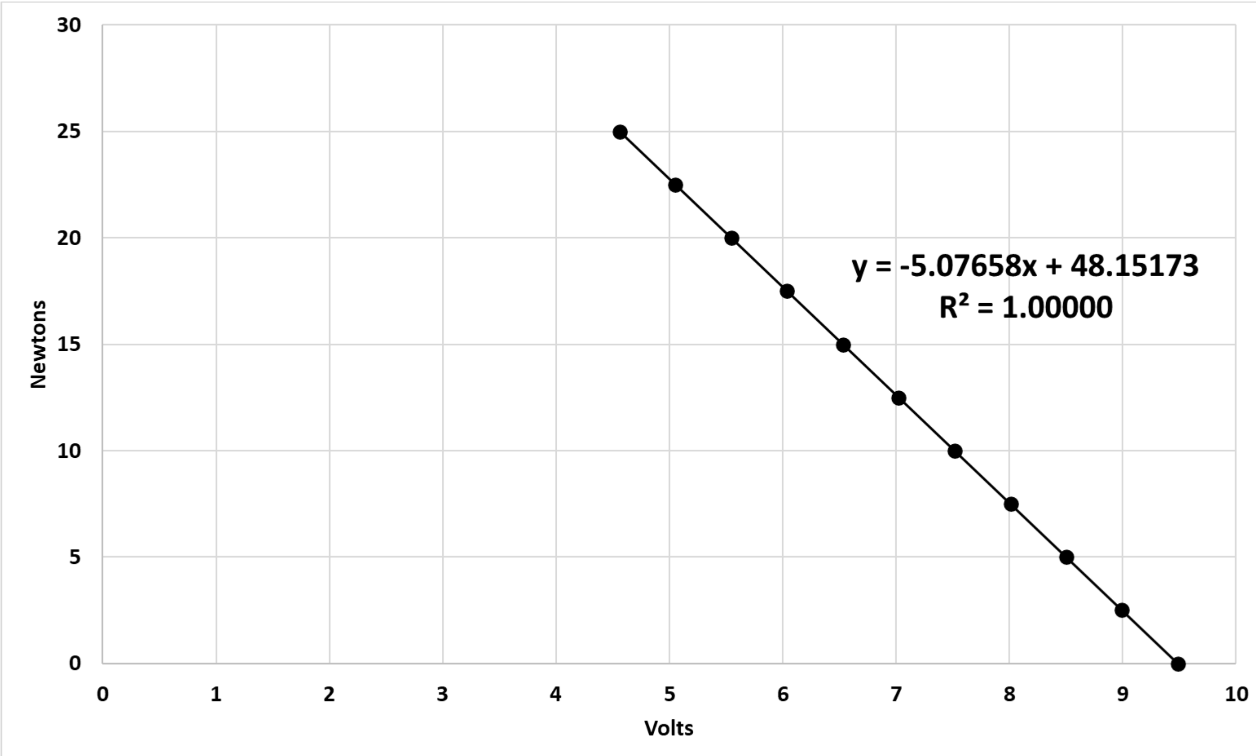

Fig. B2. Displacement DCDT calibration plot.

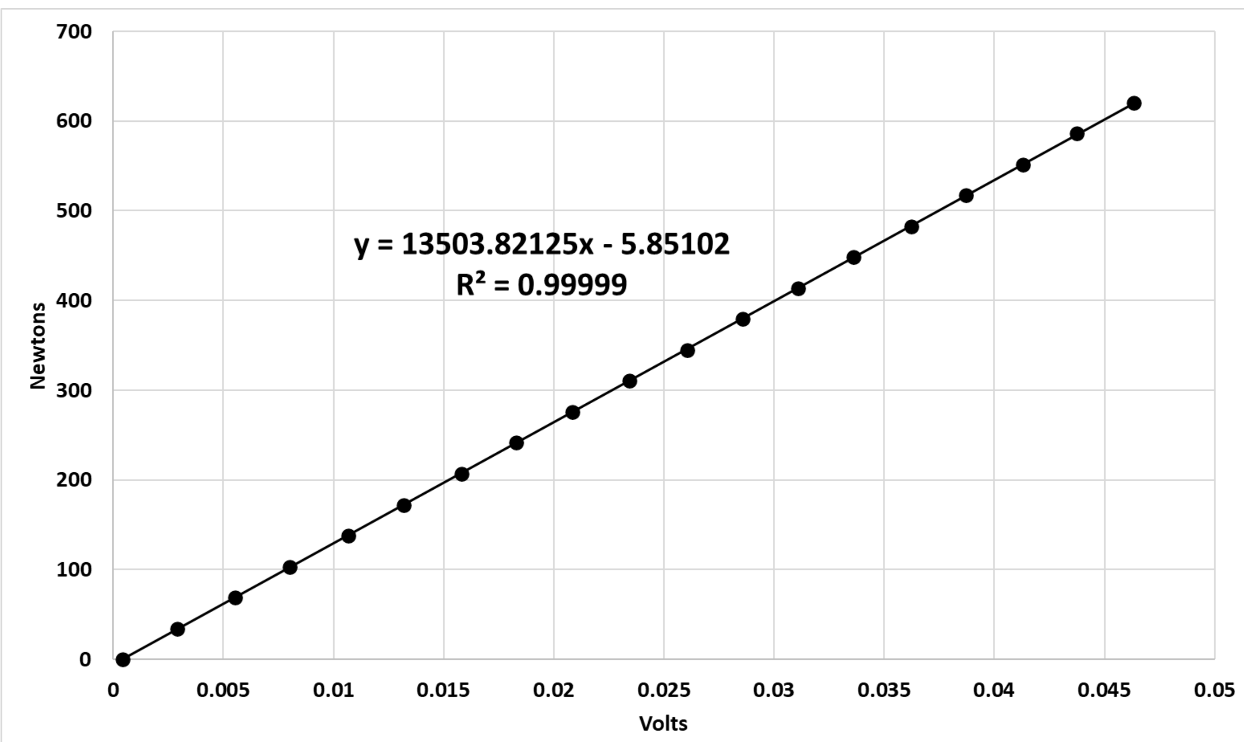

Fig. B3. Pore pressure transducer calibration plot.

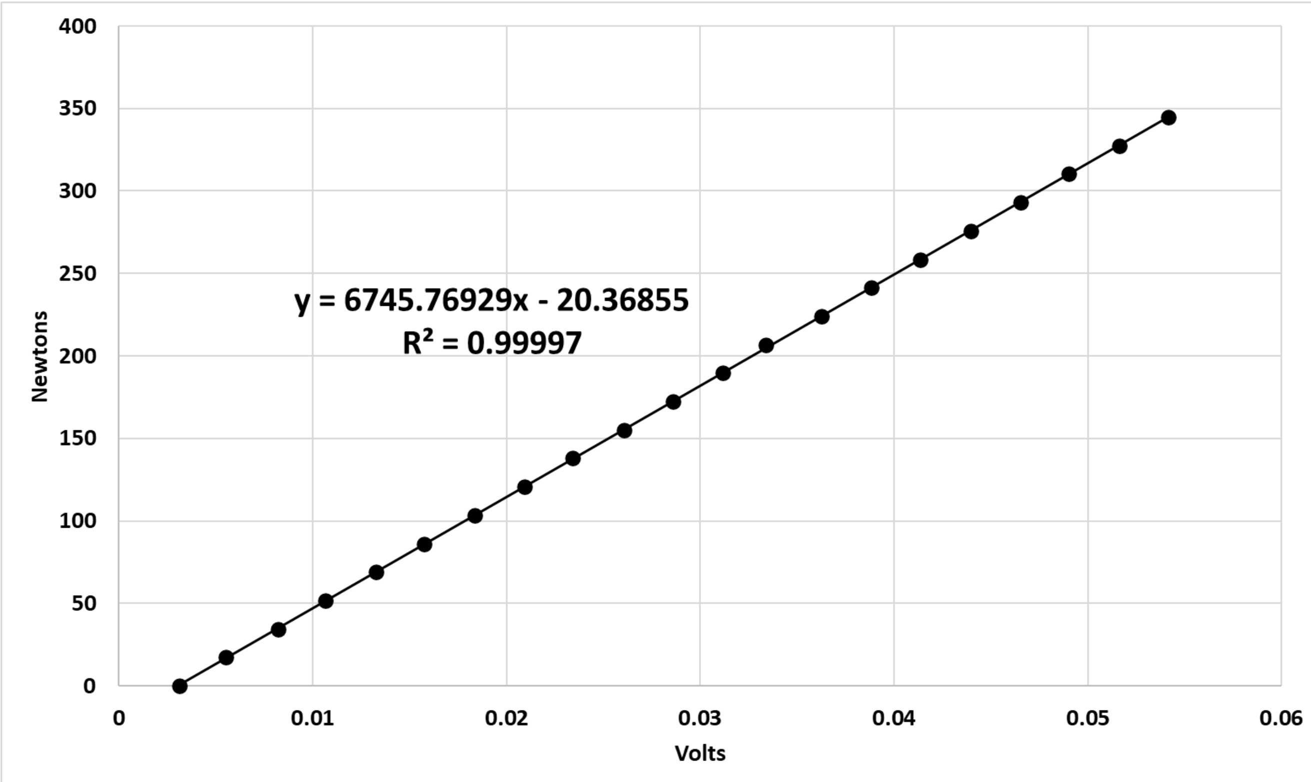

Fig. B4. Cell pressure transducer calibration plot.

APPENDIX C: Plots and Data with Peak Deviator Stress as Critical State Failure Criterion

<u>**Test 1:** 50 kPa Target Effective Stress</u>

Effective Confining Stress (kPa)	46.60
Dry Density (g/cm3)	1.33
Saturated Moisture Content	0.28
Bulk Density (g/cm3)	1.70
Void Ratio	0.74
B Parameter	0.99
Deviator Stress at Failure (kPa)	35.23
Excess Pore Pressure at Failure (kPa)	32.64
Effective Vertical Stress at Failure (kPa)	48.99
Effective Horizontal Stress at Failure (kPa)	13.75
Effective Friction Angle at Failure (deg)	34.2
Effective Undrained Shear Strength (kPa)	15.1
Axial Strain at Failure (%)	17.22

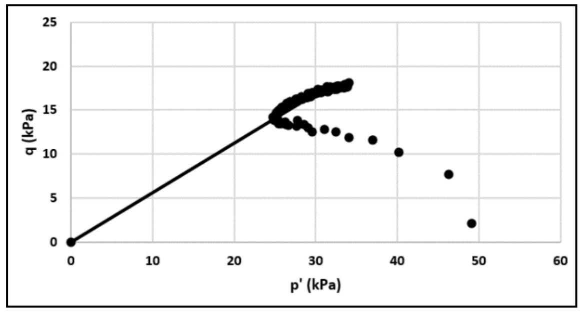

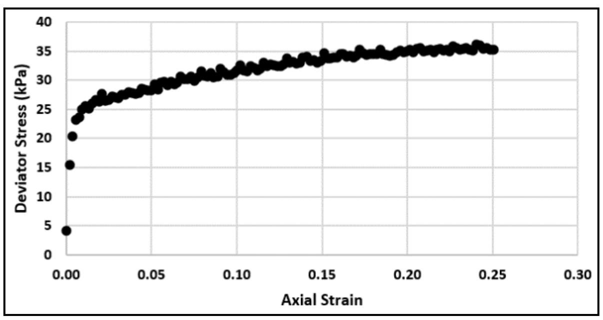

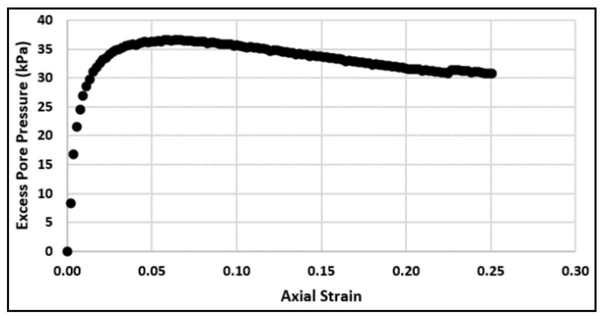

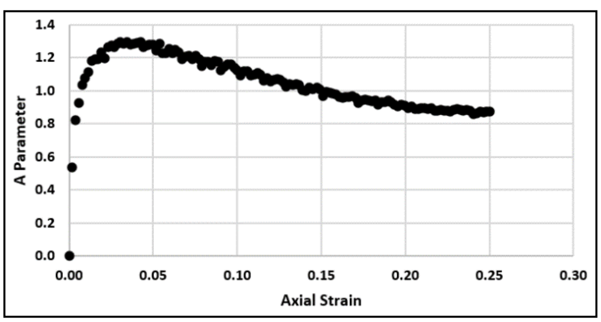

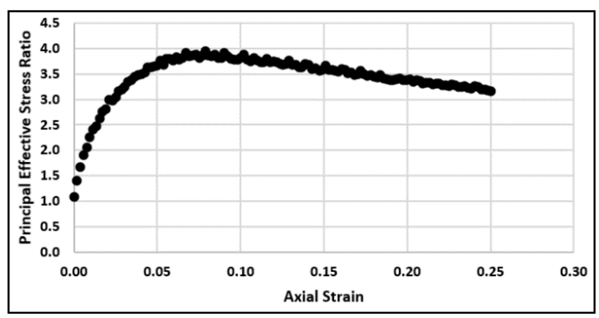

Test 2: 100 kPa Target Effective Stress

Effective Confining Stress (kPa)	96.32
Dry Density (g/cm3)	1.40
Saturated Moisture Content	0.26
Bulk Density (g/cm3)	1.76
Void Ratio	0.69
B Parameter	1.00
Deviator Stress at Failure (kPa)	72.06
Excess Pore Pressure at Failure (kPa)	61.51
Effective Vertical Stress at Failure (kPa)	106.87
Effective Horizontal Stress at Failure (kPa)	34.81
Effective Friction Angle at Failure (deg)	30.6
Effective Undrained Shear Strength (kPa)	30.9
Axial Strain at Failure (%)	18.58

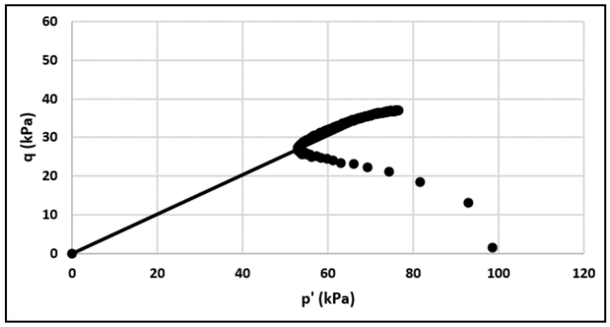

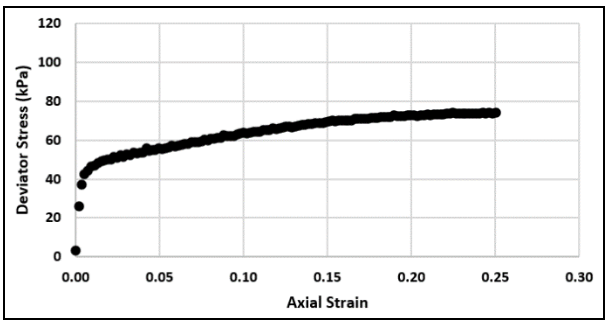

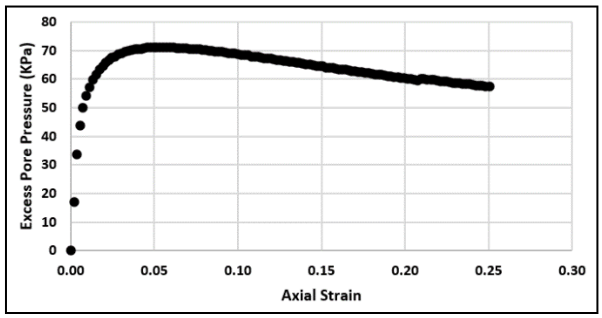

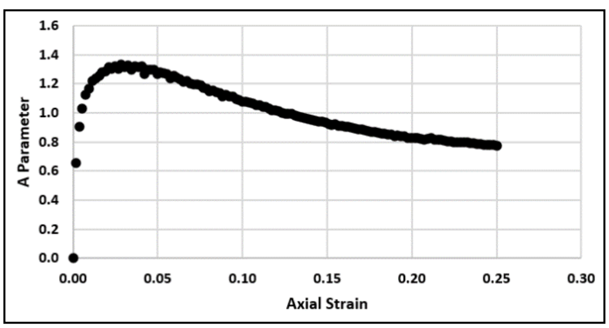

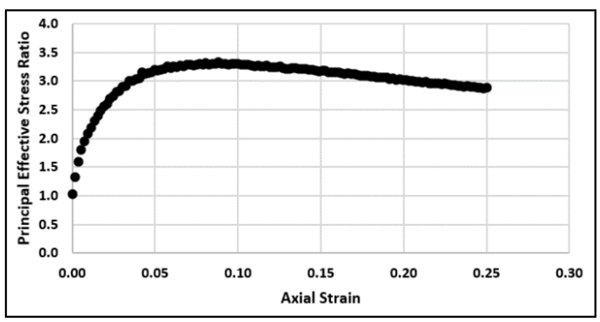

Test 3: 200 kPa Target Effective Stress

Effective Confining Stress (kPa)	193.52
Dry Density (g/cm3)	1.42
Saturated Moisture Content	0.24
Bulk Density (g/cm3)	1.77
Void Ratio	0.65
B Parameter	0.99
Deviator Stress at Failure (kPa)	153.17
Excess Pore Pressure at Failure (kPa)	115.51
Effective Vertical Stress at Failure (kPa)	231.18
Effective Horizontal Stress at Failure (kPa)	78.01
Effective Friction Angle at Failure (deg)	29.7
Effective Undrained Shear Strength (kPa)	65.7
Axial Strain at Failure (%)	20.31

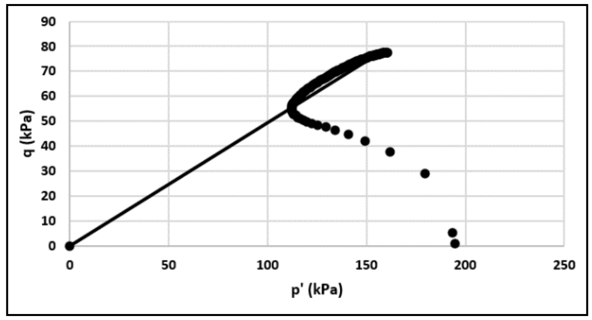

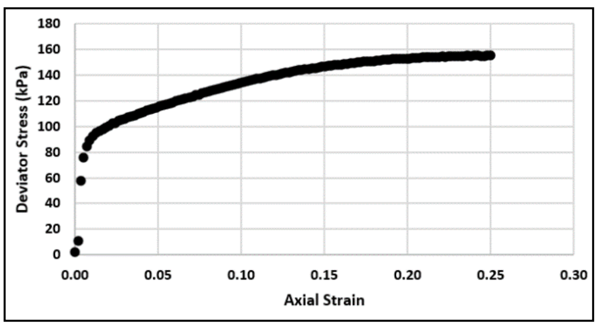

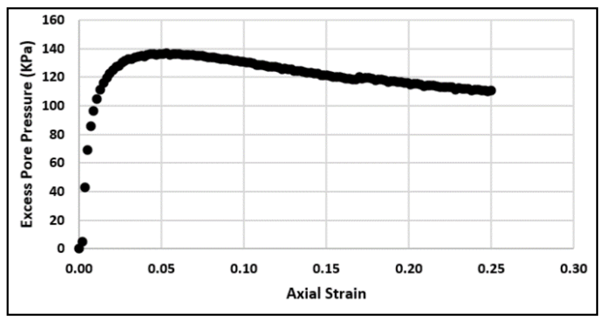

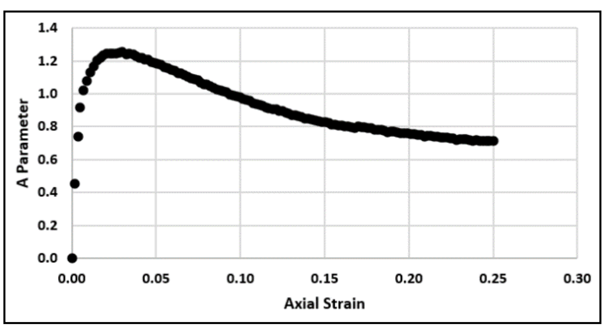

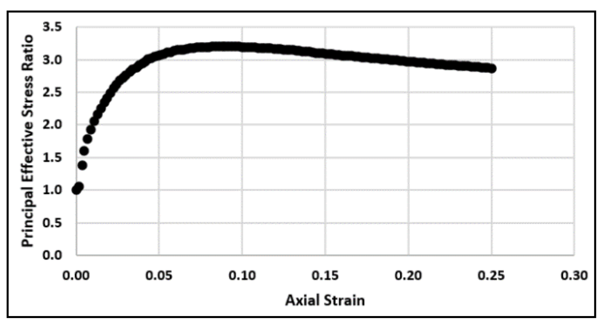

Test 4: 400 kPa Target Effective Stress

Effective Confining Stress (kPa)	396.17
Dry Density (g/cm3)	1.46
Saturated Moisture Content	0.22
Bulk Density (g/cm3)	1.79
Void Ratio	0.60
B Parameter	0.96
Deviator Stress at Failure (kPa)	308.41
Excess Pore Pressure at Failure (kPa)	237.57
Effective Vertical Stress at Failure (kPa)	467.01
Effective Horizontal Stress at Failure (kPa)	158.60
Effective Friction Angle at Failure (deg)	29.5
Effective Undrained Shear Strength (kPa)	132.2
Axial Strain at Failure (%)	21.63